JHEP PROCEEDINGS

International Europhysics Conference on HEP

Evaluation of fine pitch p–on–n and n–on–n irradiated silicon microstrip detectors for the LHCb experiment

Jim Libby* **on behalf of the LHCb collaboration**

CERN, CH-1211, Geneva 23, Switzerland

E-mail: Jim.Libby@cern.ch

Abstract: The Vertex Locator (VELO) of the LHCb experiment has to operate its silicon microstrip sensors in a harsh and non–uniform radiation environment. Irradiated prototype n–on–n and p–on–n silicon microstrip detectors have been evaluated in a test–beam while being read out at 40 MHz. Measurements of the efficiency of these prototypes are presented. The particular dangers of p–on–n detectors are outlined and the n–on–n technology choice for LHCb is motivated.

1. Introduction

The LHCb experiment is dedicated to B–physics at the Large Hadron Collider. Its goal is to use the large B-hadron statistics available to make over–constraining measurements of CP–violation in the Standard Model, and hopefully observe inconsistencies indicative of new physics contributions. Precise vertex measurements are extremely important to LHCb for two reasons. Firstly, the signature of a displaced vertex from the primary is characteristic of a B–decay, and is used in the 2nd level of the trigger to select events of interest. Secondly, excellent resolution of the B–decay time is required to make undiluted measurements of CP–violation and mixing.

The LHCb experiment instruments the forward region of one hemisphere about the pp interaction point. The pseudo-rapidity acceptance that must be covered by the Vertex Locator (VELO) is $4.9 \geq \eta \geq 1.5$. A series of 25 stations are arranged perpendicular to the beam direction over 1 m about the interaction point. Each station is divided in half so that it can be retracted during LHC injection; each half station consists of an R and a ϕ measuring sensor. More details of the VELO design can be found in [1].

2. Sensor design and radiation environment

The silicon sensor design is illustrated in Figure 1. The $R - \phi$ geometry of the strip layout gives optimal standalone tracking performance for the vertex trigger. The charge

*Speaker.

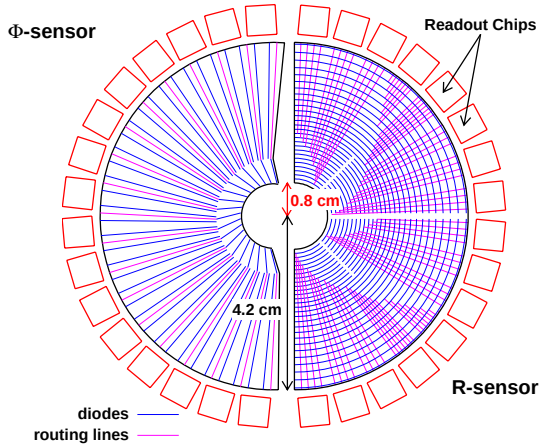

Figure 1: The layout of VELO (left) ϕ–measuring and (right) R–measuring silicon sensors.

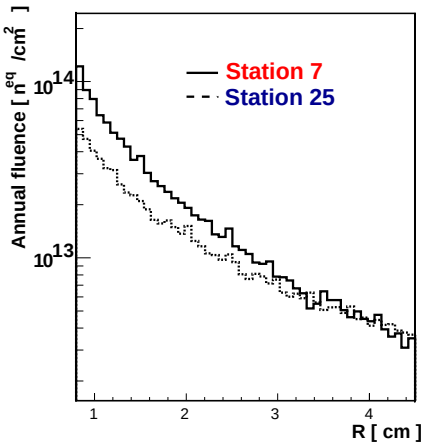

Figure 2: The fluence as a function of radius for a sensor near the interaction point (7) and the most downstream sensor (25).

collected on the implants is AC–coupled to aluminium readout strips. The ϕ sensor strips are segmented into inner and outer regions; the signals from the inner region are routed to the readout chips, at the edge of the detector, via lines in a second metal layer. The pitch at the inner radius (R =0.8 cm) is 37 μm and increases to 92 μm at the outer radius (R =4.2 cm). The pitch on the R–measuring sensors also increases with radius from 40 μm to 92 μm. All strips are read out using the routing lines in the second metal layer, which run to the outer edge of the detector crossing many strips.

The strips are subject to a non–uniform irradiation by charged particles, which depends on the radius and position relative to the interaction point as illustrated in Figure 2. The radiation varies by a factor of 30 from the inner to outer radius, with a peak value of 1.3×10^{14} $n_{\rm eq}/{\rm cm}^2$/year. Throughout this paper $n_{\rm eq}$ refers to the equivalent damage caused by neutrons of 1 MeV kinetic energy; other particle irradiations are scaled to this unit [2].

3. Prototype sensors and test–beam set–up

Prototype sensors similar to the final design have been been produced in both p–on–n and n–on–n technologies [1]. The p–on–n prototypes[1] are almost identical in strip layout to the final design illustrated in Figure 1, and the thickness of the detector was 200 μm. The n–on–n prototypes[2] have a different azimuthal coverage of 72°. However, the strip pitch and layout is similar to the final design, and a second metal layer is used for the readout. The thickness of the n–on–n prototype is 300 μm.

ϕ–measuring sensors of both types were irradiated non–uniformly in a 24 GeV beam of protons at the CERN PS [3]. The range of fluences were $(0 - 6.4) \times 10^{14}$ $n_{\rm eq}/{\rm cm}^2$ and $(0 - 2.5) \times 10^{14}$ $n_{\rm eq}/{\rm cm}^2$ for the p–on–n and the n–on–n prototypes respectively. The

[1]Manufactured by MICRON Semiconductors.
[2]Manufactured by Hamamatsu Photonics K.K.

detectors were stored and operated at -10° C to prevent any additional increases in the depletion voltage after irradiation.

The detectors were read out with SCTA128A chips [4] at 40 MHz. The irradiated detectors were placed in a beam–telescope of 4 stations of non–irradiated R and ϕ–measuring sensors of the n–on–n type, read out with VA2 chips [5]. The telescope was operated in a beam of 120 GeV pions and muons at the CERN SPS. Tracks reconstructed in the telescope have an extrapolation error of ~ 4 μm at the irradiated detectors.

4. Efficiency measurements of the prototypes

Clusters on the test detector were reconstructed with the requirement that their signal–to–noise was greater than 5 [6]. The efficiency of the prototypes was determined by extrapolating a track from the telescope and searching for a cluster within 300 μm of the intercept point. Events with only one track reconstructed in the telescope were considered.

The efficiency over the surface of the p–on–n prototype, when operated at 300 V, is illustrated in Figure 3. There are two features of note. Firstly, the region of greatest inefficiency corresponds to that of highest fluence, which is shown in Figure 4. Secondly, the inner region is more efficient than the outer for a similar fluence.

After a dose equivalent to the maximum received in one year of LHCb operation, the efficiency was 92% for the outer region of p–on–n sensor. For optimal operation of the LHCb vertex trigger, 99% efficiency is required. Furthermore, the signal–to–noise cut can not be decreased without degrading the performance due to fake clusters [7].

The effects can be explained by comparing the charge collection in a fully depleted and an underdepleted p–on–n sensor, which is represented schematically in Figure 5. The parts of the detector which are more heavily irradiated require a higher voltage to be fully depleted. At a fixed voltage, certain parts will be fully depleted, while other parts will have a non-depleted layer of differing thickness. In the fully depleted case, the charge from a particle traversing the bulk will be focused on to the p^{+}–implants of the strip, giving a narrow cluster. If the detector is underdepleted, as in the lower schematic of Figure 5,

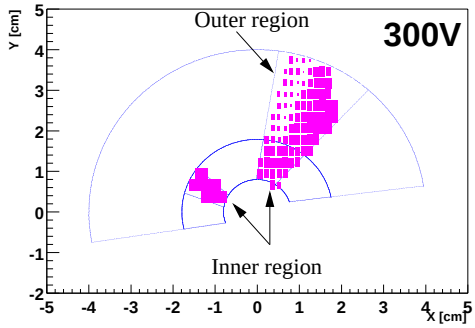

Figure 3: The efficiency of the p–on–n prototype. The efficiency is proportional to the size of the boxes.

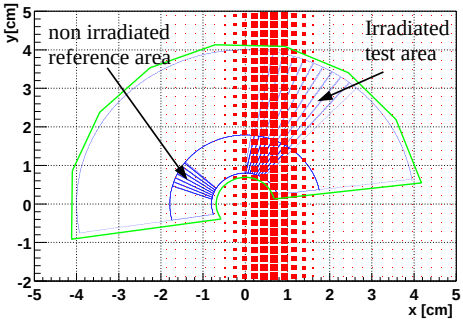

Figure 4: The map of the irradiation fluence received over the surface of the detector. The dose is proportional to the size of the boxes.

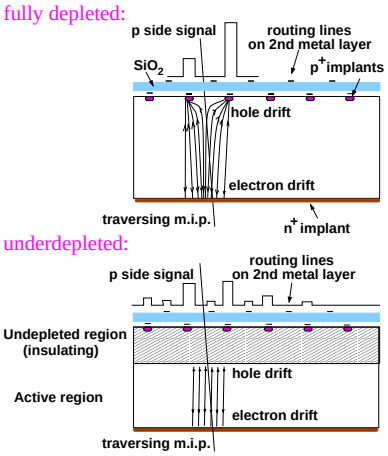

Figure 5: A schematic of the induced signal for (top) a depleted and (bottom) an underdepleted p–on–n detector.

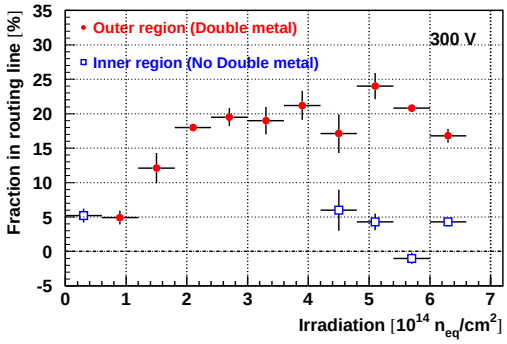

Figure 6: Fraction of charge in the routing line as a function of irradiation in the inner and outer regions on the p–on–n prototype.

there is an underdepleted layer next to the p^+ implants which acts as an insulator when AC–coupled fast electronics are used [8]. Charge from a traversing particle will only drift in the depleted region, and a mirror charge will be induced in the aluminium readout lines of several nearby strips, defocusing the cluster [9]. Furthermore, in the outer region of the p–on–n prototype detectors charge may also be induced in the routing lines in the second metal layer. These problems are not expected to occur for an underdepleted n–on–n sensor [9], where the underdepleted region is on the opposite side of the detector to the segmented n^+ implants.

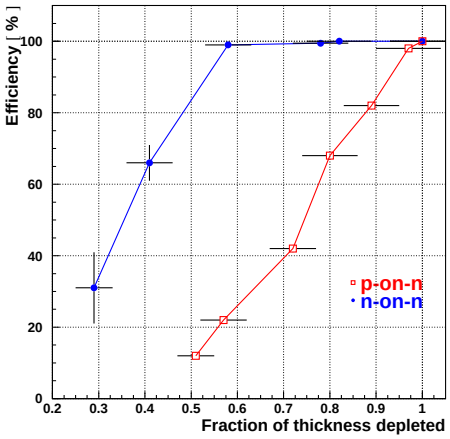

Figure 7: Comparison of p–on–n and n–on–n prototypes' efficiencies as function of the depleted depth of the detector.

The readout of the ϕ sensor is such that the adjacent channels are an outer strip and a inner strip plus routing line in the second metal layer. The charge on the strips and the adjacent readout channels about the track intercept were measured. In Figure 6 the fraction of charge on adjacent readout channels, compared to the total on the strip plus the adjacent channels, is shown as a function of the irradiation. In the inner region the maximum is $\sim 5\%$; this is the cross talk in the readout chain. In the outer region the fraction increases to over 20% for a fluence of 2.5×10^{14} $n_{\rm eq}/{\rm cm}^2$. This additional charge on adjacent channels in the outer region is that induced on the second metal layer. This charge is lost to the cluster reconstruction, which explains the decreased efficiency in the outer region.

Identical efficiency measurements were performed on the irradiated n–on–n detector. The results are given in Figure 7, along with those for the p–on–n detector. The results

are shown as a function of the fraction of the detector bulk's thickness that is depleted, $f_{\rm dep}$. This can be calculated given the measured depletion voltage, $V_{\rm dep}$, for a certain irradiation [6], and the applied voltage at which the data was taken, V, using the relation: $f_{\rm dep} = \sqrt{V/V_{\rm dep}}$. The p–on–n prototype efficiency drops as soon as there is an undepleted region in the detector; at 90% depletion the efficiency has dropped to 85%. For the n–on–n prototype the efficiency remains at 99% until less than 60% of the detector is depleted.

5. Conclusions

When LHCb is operational the non–uniform irradiation of the sensors means that at certain voltage the inner part of the detector may be underdepleted. Ideally the voltage will be raised to fully deplete the inner region, resulting in an overdepletion in the outer region. However, this may lead to problems of breakdown, or to effects such as micro–discharge noise [10], which could occur in the heavily overdepleted areas. As described in this paper, the charge spread in an underdepleted p–on–n detector leads to a lower efficiency, particularly in the presence of a second metal layer, as well as a decrease in the resolution. Therefore, the n–on–n technology was chosen for the LHCb VELO sensors.

References

[1] The LHCb Collaboration, *LHCb Vertex Locator Technical Design Report*, *CERN/LHCC* **2001-011** (2001) 1.

[2] A. Vasilescu and G. Lindstroem, *Notes on the fluence normalisation based on the NIEL scaling hypothesis*, *ROSE/TN* **2000-02** (2000) 1.

[3] J. Libby *et al.*, Measurement of the irradiation profile at the PS beam, *LHCb* **2001-020** (2001) 1.

[4] F. Aghinolfi *et al.*, *SCTA - a Rad-Hard BiCMOS Analogue Readout ASIC for the ATLAS Semiconductor Tracker*, *IEEE Trans. Nucl. Science* **44** (1997) 298.

[5] O. Toker *et al.*, *Viking, a CMOS low noise monolithic frontend for Si-strip detector readout*, *Nucl. Instrum. Meth.* **A340** (1994) 572.

[6] T. Bowcock *et al.*, *Performance of an irradiated n–on–n Hamamatsu prototype*, *LHCb* **2001-039** (2001) 1; *Performance of an irradiated p–on–n MICRON prototype*, *LHCb* **2001-040** (2001) 1.

[7] P. Koppenburg, *Simulation of the vertex trigger preprocessor: Effects of noise on L1 performance*, *LHCb* **99-003** (1999) 1.

[8] T.J. Brodbeck and A. Chilingarov, *Simulation of charge collection and sharing in microstrip detectors*, *Nucl. Instrum. Meth.* **A395** (1997) 29.

[9] K. Borer *et al.*, *Charge collection efficiency and resolution of an irradiated double–sided silicon microstrip detector operated at cryogenic temperatures*, *Nucl. Instrum. Meth.* **A440** (2000) 17.

[10] T. Ohsugi *et al.*, *Design optimisation of radiation hard, double–sided, double–metal, AC–coupled silicon sensors*, *Nucl. Instrum. Meth.* **A436** (1999) 272.